Available online at www.sciencedirect.com
ScienceDirect
Journal of Catalysis 249 (2007) 300–310
JOURNAL OF CATALYSIS
www.elsevier.com/locate/jcat

Development of stable bimetallic catalysts for carbon dioxide reforming of methane

Jianguo Zhang, Hui Wang *, Ajay K. Dalai

Department of Chemical Engineering, University of Saskatchewan, Saskatoon, Saskatchewan, S7N 5A9, Canada

Received 9 February 2007; revised 30 April 2007; accepted 6 May 2007

Available online 19 June 2007

Abstract

Using a coprecipitation method to form Ni–Me–Al–Mg–O composite, Ni–Me (Me = Co, Fe, Cu, or Mn) bimetallic catalysts were prepared for carbon dioxide reforming of methane. Catalyst screening with the reforming reaction showed that Ni–Co bimetallic catalyst had superior performance in terms of activity and stability to other Ni–Me combinations. In a 2000 h stability test under the conditions of 750 °C, 1 atm, and GHSV of 110,000 mL/g_{cat}-h (0.05 g of catalyst and 5.5 L/h gas flow rate), Ni–Co catalyst showed very stable performance with very low carbon formation. Reducing Ni and Co content from 6.1 and 9.3 to 3.6 and 4.9 mol% (metal base), respectively, rendered to completely eliminate carbon deposition for up to 250 h. Catalyst characterization was conducted using ICP-MS, BET, XRD, H_2-TPR, CO_2-TPD, CO-chemisorption, TEM, and TG. It is believed that the synergy between Ni and Co can significantly improve catalyst performance and reduce carbon formation. A high metal dispersion or small ensemble size can be enhanced by reducing the Ni–Co content. The high activity and excellent stability of Ni–Co catalyst was closely related to its high metal dispersion, strong metal–support interaction, and formation of stable solid solutions.

Keywords: CO_2 reforming of CH_4; Bimetallic catalyst; Nickel; Cobalt; Alumina; Magnesium oxide; Coprecipitation

1. Introduction

Carbon dioxide reforming of methane (also known as dry reforming) to produce synthesis gas is becoming more research-attractive due to the increasing interest in reduction of carbon dioxide emissions and more efficient utilization of natural gas. As shown in Eq. (1), the major greenhouse gas, CO_2, can be converted into valuable synthesis gas through the reforming reaction of methane,

$$CH_4 + CO_2 = 2CO + 2H_2, \quad \Delta H^0_{298\ K} = 247\ \text{kJ/mol}. \qquad (1)$$

With a H_2/CO ratio of unity, the synthesis gas such produced is a desired feedstock for synthesis of oxygenates [1,2]. The combination of dry reforming and steam reforming can produce synthesis gas with the ideal ratio of H_2/CO for the Fischer–Tropsch synthesis [3],

$$CH_4 + H_2O = CO + 3H_2, \quad \Delta H^0_{298\ K} = 206\ \text{kJ/mol}. \qquad (2)$$

Due to its highly endothermic property, CO_2 reforming of CH_4 also has desirable thermodynamic characteristics of a chemical energy transmission system (CETS) [4–8].

Carbon dioxide reforming of methane was first studied by Fischer and Tropsch over a number of base metal catalysts [3]. It is well known that this reaction can be catalyzed by all VIII transition metals except osmium. Noble metals, such as ruthenium (Ru) and rhodium (Rh), and the nonnoble metal nickel (Ni) have been studied extensively for this reaction [9–12]. It has been found that supported Rh, Ru, Pd, Pt, and Ir catalysts can provide stable operations for carbon dioxide reforming of methane with low carbon formation or deposition on the catalysts during the reaction [13]. However, from an industrial standpoint, it is more practical to develop nonnoble metal-based catalysts to avoid the high cost and restricted availability of noble metals. Ni has drawn significant research attention due to its high activity and wide availability [14]. The great challenge for Ni catalysts is that they suffer severe catalyst deactivation due to sintering, metal oxidation [15], and especially significant carbon formation [13,14,16].

* Corresponding author. Fax: +1 306 966 4777.
E-mail address: hui.wang@usask.ca (H. Wang).

0021-9517/$ – see front matter
doi:10.1016/j.jcat.2007.05.004

Consequently, many attempts have been made to suppress carbon formation over Ni-based catalysts when studying carbon dioxide reforming of methane. Ruckenstein and Hu [17,18] reported that NiO/MgO has excellent stability and good resistance to carbon formation because of the formation of a solid solution between NiO and MgO, which is believed to suppress CO disproportionation. Tomishige et al. [19] investigated the effect of Sn, Ge, and Ga to a NiO–MgO solid solution and found that the addition of Sn can effectively decrease the carbon formation, resulting mainly from methane decomposition. The addition of Cr [20,21] and Mn [22] reportedly had significant effects on the inhibition of carbide formation, which is believed to be the intermediate for carbon formation [23]. Choudhary and Mamman [24] reported that catalyst performance can be improved when partial NiO is replaced with CoO in the NiO–MgO solid solution. Takanabe et al. [25] reported that a homogeneous alloy of Co and Ni and low Ni substitution of Co dramatically improved catalyst activity and stability. They ascribed the enhanced performance to the improved catalyst resistance to metal oxidation. In summary, it is clear that bimetallic catalysts may exhibit superior performance for carbon dioxide reforming of methane compared with the corresponding monometallic catalysts [26,27]. Considerable research also has been conducted on the modification of catalyst supports using promoters [28–33] to overcome the deactivation associated with nickel-based catalysts. It was reported that the addition of K and Ca can significantly inhibit carbon formation due to the favorable adsorption of acidic CO_2 on the basic surface sites [34,35]. Catalyst surface basicity is believed to help suppress carbon deposition by promoting the activation of CO_2 [36,37] on the surface of catalysts. However, catalyst deactivation remains a serious problem for carbon dioxide reforming of methane.

This work applies a new approach of incorporating different properties that are believed to improve performance and stability into one system aiming at solving the deactivation problem of Ni-based catalyst for CO_2 reforming of CH_4. In the designed catalyst reported in this paper, the sintering was supposed to be inhibited or eliminated through improved catalyst thermal stability by using a material with a high melting point, MgO. The catalyst activity was supposed to be improved by providing high contact area using a material with high surface area, Al_2O_3. The synergy of metal–metal was assumed to improve performance by reducing the possibility of metal oxidation. A high-temperature calcination pretreatment process was proposed to improve the metal–support interaction to reduce carbon formation. Thus, it was assumed that high metal dispersion, high surface area, and SMSI could be incorporated into a Ni–Me bimetallic catalyst. Catalyst screening showed that the Ni–Co bimetallic catalysts had high activity and stability for carbon dioxide reforming of methane. Carbon-free operation was achieved in a 250-h stability experiment.

2. Experimental

2.1. Catalyst preparation

Ni–Co bimetallic catalyst was prepared by coprecipitating a common aqueous solution of nickel nitrate (98% purity; Lancaster Synthesis), cobalt nitrate (99% purity; Aldrich), magnesium nitrate (EMD Chemicals), and aluminum nitrate (EMD Chemicals). Other bimetallic catalysts were prepared by replacing cobalt nitrate with $Fe(NO_3)_3{\cdot}9H_2O$ (99% purity, Lancaster Synthesis), $Mn(NO_3)_2{\cdot}xH_2O$ (99.98% purity; Lancaster Synthesis), and $Cu(NO_3)_2{\cdot}6H_2O$ (99% purity; Aldrich), respectively. The precipitate was washed using deionized water 2 or 3 times, dried overnight in the air at 120 °C, and then calcined in the air at 900 °C for 6 h. The prepared catalysts were designated Ni–Me–Al–Mg–O (where Me = Co, Fe, Cu, or Mn). Here we designate these catalysts as Ni–Co, Ni–Fe, Ni–Cu, and Ni–Mn, respectively.

2.2. Catalyst characterization

The metal composition of the catalysts was analyzed at the Saskatchewan Research Council Analytical Laboratory using inductively coupled plasma mass spectrometry (ICP-MS). The results are given in Tables 1 and 2. Metal compositions are used because they were measured directly and they do not change after catalyst reduction. Oxygen in the catalyst composite is stoichiometrically balanced.

The surface composition of same samples was analyzed using X-ray photoelectron spectroscopy (XPS) in the Department of Chemical and Materials Engineering at the University of Alberta. The results are shown in Table 2.

The BET surface area, porous volume, and average pore diameter of the catalysts were measured by N_2 adsorption at the temperature of −196 °C using a Micromeritics ASAP 2000. Approximately 0.2 g of catalyst was used for each analysis. The degassing temperature was 200 °C, to remove the moisture and other adsorbed gases from the catalyst surface. Some of the results are given in Tables 1 and 3.

The metal dispersion and metal surface area were determined by CO chemisorption. The sample was first reduced us-

Table 1
Elemental composition, BET surface area, average pore diameter of different bimetallic catalysts

Catalyst	Metal elemental composition (MEC)[a] (mol%)							BET surface (m^2/g)	Pore volume (ml/g)	Average pore diameter (nm)
	Ni	Fe	Cu	Mn	Co	Al	Mg			
Ni–Fe	6.5	7.9	–	–	–	29.0	56.6	18	0.0565	12.0
Ni–Cu	6.8	–	6.9	–	–	28.6	57.7	15	0.0881	19.6
Ni–Mn	6.0	–	–	9.0	–	27.8	57.1	17	0.0734	16.9
Ni–Co	6.1	–	–	–	9.3	28.2	56.4	54	0.160	10.4

[a] MEC was measured by inductively coupled plasma mass spectrometry. O should be stoichiometrically balanced in the catalyst composites.

Table 2
Elemental composition of Ni and Co monometallic and Ni–Co bimetallic catalysts

Catalyst	Bulk metal composition (mol%)				Surface metal composition (mol%)			
	Ni	Co	Al	Mg	Ni	Co	Al	Mg
Ni	6.8	–	27.8	65.4	7.1	–	28.9	64.0
Co	–	9.7	27.6	62.8	–	7.8	31.2	61.0
Ni–Co (L)[a]	3.6	4.9	30.0	61.5	4.3	6.2	29.3	60.2

[a] L denotes the low Ni–Co content in comparison with the Ni–Co catalyst in Table 1.

Table 3
BET surface area, average pore diameter, metallic surface area, and metal dispersion of Ni and Co monometallic and Ni–Co (L) bimetallic catalysts

Catalyst	BET surface (m^2/g)	Pore diameter (nm)	Metallic surface (m^2/g)	Metal dispersion (%)
Ni	45	9.0	1.2	2.9
Co	24	10.5	1.5	2.1
Ni–Co (L)	56	8.5	2.9	8.8
Ni–Co	54	10.4	4.1	7.5

ing hydrogen at 850–900 °C for 4 h. The reduced sample was moved to a sample holder under the protection of the inert gas (He). Three steps were carried out before CO chemisorption using a Micromeritics ASAP 2000: (1) evacuating the sample for 30 min at 120 °C, (2) reducing the sample again at 450 °C for 30 min using H_2, and (3) evacuating the sample for another 30 min at 120 °C. Finally, CO chemisorption was conducted at 35 °C. The results of some samples are listed in Table 3.

X-ray powder diffraction (XRD) analysis was conducted using a Rigaku/Rotaflex Cu rotating anode X-ray diffraction instrument. The catalyst was powdered and mixed with methanol to form a mud, which was loaded to the coarse side of a glass plate and placed under the ambient drying conditions. The dried sample plate was then loaded in the analysis chamber. Each sample was scanned at a rate of 4°/min with 2-Theta varying from 20 to 80°.

The reducibility of catalysts was studied in a quartz tube by temperature-programmed reduction (TPR) in Chembet-3000. A sample of about 0.1 g of was heated from room temperature to 1000 °C using 3% H_2/N_2 at a flow rate of 30 mL/min and a ramp rate of 5 °C/min.

The carbon deposition was analyzed using a Perkin–Elmer Pyris Diamond TG/DTA instrument. The spent catalyst was heated in a platinum sample holder in the air from room temperature to 850 °C at a ramp rate of 5 °C/min. Transmission electron microscopy (TEM) was used to investigate the morphology of carbon deposits on the spent catalysts.

2.3. Catalyst testing

The evaluation of catalysts was carried out in a benchtop fixed-bed quartz microreactor (Autoclave) with an i.d. of 6 mm. In screening of different bimetallic combinations and 2000 h stability test for Ni–Co catalyst, 0.05 g of catalyst was diluted with 0.450 g of quartz sand. To compare the selected catalysts at lower conversions, less catalyst and the same gas flow rate were used so as to maintain the comparison in the same mass transfer regime. To investigate the effects of Ni and Co content, 0.03 g of catalyst was mixed with 0.470 g of quartz sand. 0.025 g of catalyst mixed with 0.475 g of quartz sand was applied in the comparison between bimetallic and monometallic catalysts. The average catalyst particle size is 0.165 mm. All experiments were carried out at 750 °C and 1 atm, and feed flow rate $F = 5.5$ L/h. No temperature gradient was observed cross the catalyst bed. Based on literature [38,39], mass transfer was mostly eliminated at such conditions of high flow rate and small amount of catalyst with small particle sizes. However, to make valid comparison on the same basis, exactly the same reaction conditions were applied in each comparison. Reactant gas consisting of an equimolar mixture of N_2 (99.9% purity, Praxair Canada Inc.), CH_4 (99.2% purity, Praxair Canada Inc.) and CO_2 (99.9% purity, Praxair Canada Inc.) was introduced at the atmospheric pressure. Before testing, the catalyst was reduced by a H_2 (99.9% purity, Praxair Canada Inc.) and N_2 mixture with a molar ratio of 1:4 at 850–900 °C for 4 h. The product gas was analyzed by an on-line Agilent 6890N GC, equipped with TCD and a GS-GasPro capillary column (J&W Scientific) of 60 m in length and 0.32 mm in inner diameter. Helium (ultra high purity 5.0, Praxair Canada Inc.) was used as the carrier gas. The GC oven temperature in analysis was initially held at −60 °C for 3 min and then was increased to 30 °C at a 25 °C/min ramp rate.

3. Results and discussion

3.1. Catalyst design and screening

3.1.1. Thermodynamics of carbon dioxide reforming of methane

Carbon dioxide reforming of methane is a highly endothermic reaction (Eq. (1)). Thermodynamic calculation indicates that the reforming reaction (Eq. (1)) at 1 atm pressure is not spontaneous (i.e., $\Delta G > 0$) below 633 °C. However, at high temperatures where the reforming reaction is spontaneous, the other four side reactions (Eqs. (3)–(6)) may occur, which will have a significant impact on the target reaction (Eq. (1)) [40].

$$CH_4 = C + 2H_2, \quad \Delta H^0_{298\ K} = 75\ \text{kJ/mol}, \tag{3}$$

$$2CO = C + CO_2, \quad \Delta H^0_{298\ K} = -171\ \text{kJ/mol}, \tag{4}$$

$$CO + H_2 = C + H_2O, \quad \Delta H^0_{298\ K} = -131\ \text{kJ/mol}, \tag{5}$$

$$CO_2 + H_2 = CO + H_2O, \quad \Delta H^0_{298\ K} = 41\ \text{kJ/mol}. \tag{6}$$

Fig. 1 shows the variation of equilibrium constants of the reactions involved as a function of temperature. For a strong endothermic reaction, the equilibrium constant of Eq. (1)

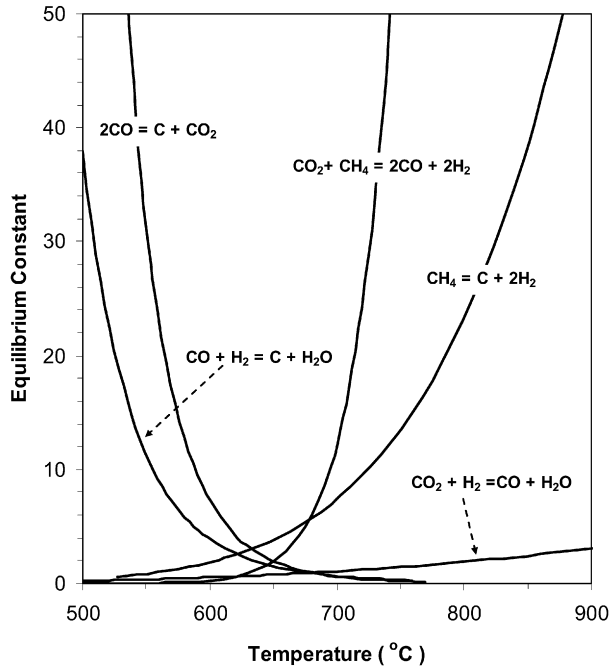

Fig. 1. Equilibrium constants of reactions (Eqs. 1, (3)–(6)) as a function of temperature.

increases dramatically with increasing reaction temperature. Thus, high conversion is favored at high temperatures. The equilibrium constants of the moderate endothermic reactions, methane decomposition (Eq. (3)), and the reverse water-gas shift reaction (RWGS; Eq. (6)), also increase with temperature. The two carbon deposition reactions, the Boudouard reaction (Eq. (4)) and the reverse carbon gasification reaction (Eq. (5)), are exothermic and thermodynamically unfavorable at high temperatures. Therefore, high reaction temperatures (i.e., 750 °C and above) are more favorable to increasing the equilibrium conversion of the target reaction (Eq. (1)) than that of the side reactions (Eqs. (3)–(5)).

3.1.2. Selection of catalyst component

Ni catalysts are prone to carbon formation, especially at high reaction temperature, which is the major cause of catalyst deactivation during carbon dioxide reforming of methane [15,41,42]. Catalyst sintering is another cause of catalyst deactivation [15]. From the thermodynamic standpoint, as discussed earlier, a high reaction temperature must be chosen to achieve high reactant conversion. However, at high temperatures, the active metal crystallites in the catalysts contact each other through thermal motion. Even at the Hutting temperature (0.3 times the melting point of the substance), the surface atoms would have sufficient energy to overcome the weak surface crystal forces, then diffuse and form necks to decrease the surface energy [43]. In this work, the catalysts were designed so as to overcome the catalyst deactivation problems. A second metal active component was applied to improve carbon resistance. The second metal was selected from Co, Fe, or Cu because Ni, Co, Fe, and Cu have similar electronic configurations. Mn was also selected because it is a proven promoter able to suppress carbon formation [29,44]. As for the framework material of the catalyst, MgO was selected because of its high melting point (3073 °C) that is able to pose resistance to sintering. However, MgO has the drawback of low specific surface area. To compensate, Al_2O_3 was added, thus, a mixed framework of $AlMgO_x$ was to be formed which would simultaneously has the high thermal stability of MgO and high specific surface area of Al_2O_3.

Based on the aforementioned consideration, a series of Ni-based bimetallic catalysts with different combinations of Ni–Co, Ni–Mn, Ni–Fe, and Ni–Cu in the framework of $AlMgO_x$ were prepared by the coprecipitation method. The level of metal content was first determined based on the relevant literature [45]. For convenience, the catalysts were denoted as Ni–Co, Ni–Mn, Ni–Fe, and Ni–Cu, respectively. The elemental composition (metal base), surface area, porous volume, and average pore diameter are shown in Table 1. The Ni–Fe, Ni–Cu, and Ni–Mn catalysts had the same level of BET surface area at 14–18 m^2/g. Meanwhile, the Ni–Co catalyst had a significantly higher surface area, 53 m^2/g. The porous volume followed the order Ni–Co $\gg$ Ni–Cu > Ni–Mn > Ni–Fe, and the average pore diameter followed the order Ni–Co < Ni–Fe < Ni–Mn < Ni–Cu. The BET analysis indicated a significant difference between the Ni–Co combination and the other combinations.

3.1.3. Screening of catalysts for carbon dioxide reforming of methane

The activity and stability within a 28-h period was investigated over 0.05 g of catalyst at 750 °C, 1 atm, $F = 5.5$ L/h, and $CH_4/CO_2/N_2 = 1/1/1$. At this reaction condition, the equilibrium conversion of CH_4 was 91.5%. The catalyst activity in terms of CH_4 conversion is shown in Fig. 2a. Ni–Co catalyst had a high initial activity (91.4% CH_4 conversion) and remained at this level throughout the 28 h of time on stream (TOS). Ni–Mn and Ni–Fe catalysts also had high initial activities, with CH_4 conversion of 85 and 53%, respectively; however, the conversion dropped to 63 and 18%, respectively, at the end of the 28-h testing period. Ni–Cu showed low but relative stable activity, with a CH_4 conversion <16%. The initial activity follows the order Ni–Co > Ni–Mn > Ni–Fe > Ni–Cu. This order is in agreement with the order of the BET surface area, porous volume, and average pore diameter (Table 1). The selectivity results in terms of H_2/CO ratio, shown in Fig. 2b, reflect no obvious difference among the different bimetallic catalysts.

After reaction, the amount of carbon formed on the catalysts was analyzed using TG/DTA. The average rate of carbon deposition is shown in Fig. 3. Clearly, the Ni–Fe catalyst had a high carbon deposition rate of 0.02104 g_c/g_{cat}-h. Correspondingly, it had a 67% activity decay (calculated on the basis of initial and final CH_4 conversion). Ni–Mn catalyst also had a relatively high carbon formation rate of 0.00543 g_c/g_{cat}-h and an activity decay of 26%. However, Ni–Cu catalyst had a lower carbon formation rate of 0.00222 g_c/g_{cat}-h and a relatively stable performance, with an activity decay of 22%. Ni–Co catalyst had the lowest carbon formation rate, 0.00204 g_c/g_{cat}-h. Meanwhile, it had a very stable performance in the 28-h period

with no activity decay. The activity decay followed the same order as the carbon formation rate: Ni–Fe ≫ Ni–Mn > Ni–Cu > Ni–Co (Fig. 3). This indicates that carbon formation is the main cause of catalyst deactivation in carbon dioxide reforming of methane. Ni–Co and Ni–Cu catalysts both exhibited good carbon resistance, but the former had much higher activity.

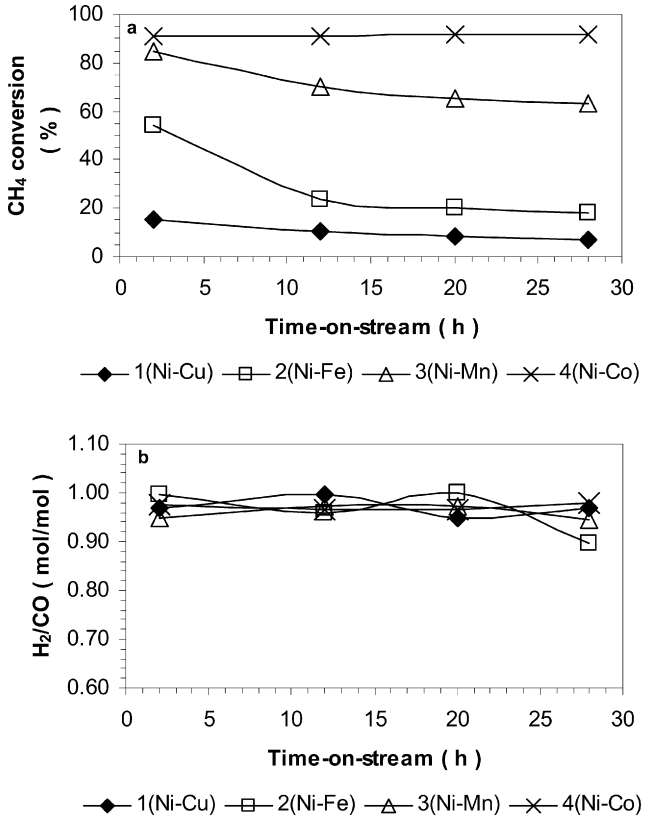

Fig. 2. Stability of different bimetallic catalysts at reaction conditions: $T = 750\,^{\circ}C$, $P = 1$ atm, $F = 5.5$ L/h, $CH_4/CO_2/N_2 = 1/1/1$, 0.05 g catalyst. (a) CH_4 conversion as a function of time-on-stream; (b) H_2/CO as a function of time-on-stream.

3.1.4. Long-term stability and carbon formation of Ni–Co bimetallic catalyst

Catalyst screening shows that Ni–Co did not lose its activity during the 28-h test, but the carbon deposition observed may affect its long-term performance. Therefore, the long-term stability and carbon formation behavior of Ni–Co catalyst were investigated to gain insight into the relationship between the carbon formation and the catalyst deactivation. At the conditions of 750 °C, 1 atm, $F = 5.5$ L/h, and $CH_4/CO_2/N_2 = 1/1/1$, Ni–Co catalyst was tested for 20, 200, and 2000 h, respectively. The results of the reaction rate of CH_4 and the amount of carbon deposition are shown in Fig. 4. The use of a common logarithm of time (h) shows more detail for the first 200 h. In the 20-h test, the reaction rate of CH_4 was maintained at around 0.000415 mol/g_{cat}-s, but the amount of carbon formed was 0.0408 g_c/g_{cat}. In the 200-h test, the CH_4 reaction rate was maintained at 0.000416 mol/g_{cat}-s for 100 h but dropped to 0.000409 mol/g_{cat}-s at 200 h. Over the 200-h test period, 0.2374 g_c/g_{cat} of carbon was formed. In the 2000-h test, the CH_4 reaction rate began to drop at 100 h from the ini-

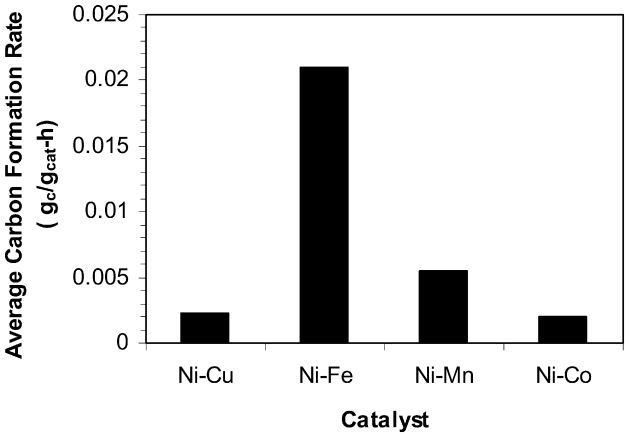

Fig. 3. Average carbon formation rate of different bimetallic catalysts within 28 h time-on-stream at reaction conditions: $T = 750\,^{\circ}C$, $P = 1$ atm, $F = 5.5$ L/h, $CH_4/CO_2/N_2 = 1/1/1$, 0.05 g catalyst.

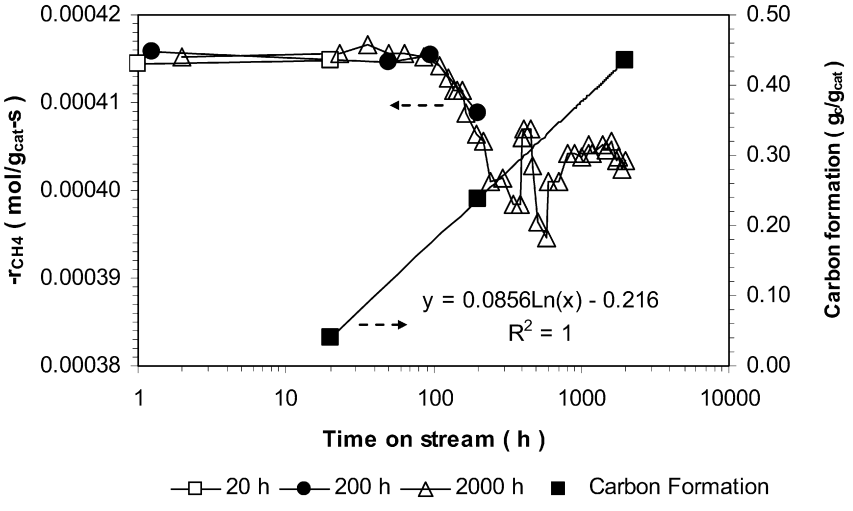

Fig. 4. Carbon formation and reaction rate of methane as a function of time-on-stream over Ni–Co catalyst at reaction conditions: $T = 750\,^{\circ}C$, $P = 1$ atm, $F = 5.5$ L/h, $CH_4/CO_2/N_2 = 1/1/1$, 0.05 g catalyst.

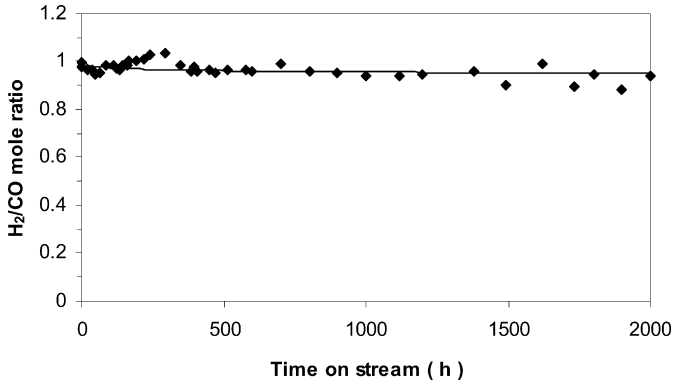

Fig. 5. H_2/CO as a function of time-on-stream over Ni–Co catalyst at reaction conditions: $T = 750\,^{\circ}C$, $P = 1$ atm, $F = 5.5$ L/h, $CH_4/CO_2/N_2 = 1/1/1$, 0.05 g catalyst.

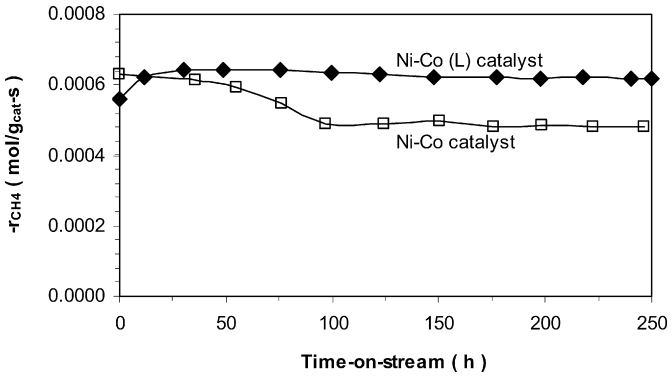

Fig. 6. Activity and stability of different Ni–Co content bimetallic catalysts at reaction conditions: $T = 750\,^{\circ}C$, $P = 1$ atm, $F = 5.5$ L/h, $CH_4/CO_2/N_2 = 1/1/1$, 0.03 g catalyst.

tial 0.000415 to 0.000398 mol/g_{cat}-s at about 300 h, fluctuated between 0.000395 and 0.000407 mol/g_{cat}-s until 700 h, and stayed stable at 0.000404 mol/g_{cat}-s for the last 1300 h. The amount of carbon formed was 0.435 g_c/g_{cat} over the 2000-h period. It can be seen that the carbon formation over Ni–Co catalyst has a very clear relationship with TOS; regression shows that this relationship is as follows:

carbon formation amount:

$$g_c/g_{cat} = 0.0856 \log(\text{TOS, h}) - 0.216. \quad (7)$$

Carbon accumulation becomes significantly slower with increasing TOS. The average carbon formation rate is 0.00204, 0.00119, and 0.000218 g_c/g_{cat}-h for the 20, 200, and 2000 h runs, respectively. Further treatment produced average carbon formation rates of 0.00204 g_c/g_{cat}-h for the first 20 h of TOS, 0.00109 g_c/g_{cat}-h for the next 180 h, and 0.000109 g_c/g_{cat}-h for the last 1800 h. It is speculated that the rapid carbon formation during the first 100 h leads to the obvious catalytic activity decline in the subsequent 200-h period. The later slowed carbon formation results in stable performance. Overall, catalytic activity for the Ni–Co bimetallic catalyst decreased by <3% over the 2000-h period. This catalyst can be claimed to be the most stable that has ever been developed for CO_2 reforming of CH_4.

The ratio of H_2/CO as a function of TOS is shown in Fig. 5. RWSR is the major side reaction in the methane dry-reforming system [13]. Its existence will reduce the H_2/CO ratio. The average ratio of H_2 to CO over this catalyst was about 0.965, which may indicate the occurrence of RWSR but of less significance. It is also interesting to note that the molar ratio of H_2 to CO oscillates between 0.9 and 1.1 during the reaction period. Wei et al. [46] ascribed this phenomenon to a periodic cycle of carbon deposition and elimination. An efficient periodic cycle of carbon deposition and elimination on the catalyst surface may be one of the contributions leading to stable catalytic performance [43].

3.1.5. Effects of the Ni–Co content in bimetallic catalysts

Although Ni–Co bimetallic catalyst showed good stability for carbon dioxide reforming of methane and good carbon resistance, further attempts to adjust the metal loading were made to eliminate carbon formation over catalyst. The work was inspired by Ruckenstein et al. [47], who reported that the lower metal loading catalyst had better carbon resistance. Based on this consideration, a Ni–Co bimetallic catalyst of nearly half of the Ni and Co loading, namely Ni–Co (L), was prepared. Its composition is shown in Table 2. The stability experiments for both Ni–Co (L) and Ni–Co were carried out over 0.03 g of catalyst at 750 °C, 1 atm, $F = 5.5$ L/h, and $CH_4/CO_2/N_2 = 1/1/1$. Because the catalyst activity was high, less catalyst was used for an effective comparison. Fig. 6 shows that the Ni–Co (L) catalyst had obviously better stability than the Ni–Co catalyst. The initial CH_4 reaction rate over the Ni–Co (L) catalyst was slightly lower than that over the Ni–Co catalyst. However, the CH_4 reaction rate over the Ni–Co (L) catalyst increased with TOS and remained at the same level even after 250 h. Similar findings also were reported by Ruckenstein et al. [45] and Zhang et al. [48,49]. This behavior was ascribed to the formation of new active sites when the catalyst was exposed to the reaction mixture [48–50]. TG/DTG analysis on the two spent catalysts with different Ni–Co contents indicated that no detectable carbon was formed on Ni–Co (L) catalyst but carbon was detected on the Ni–Co catalyst (Figs. 7a and 7b). The TEM analysis (Fig. 8a) further confirmed that no carbon was formed on the spent Ni–Co (L) catalyst. Fig. 7b shows that two kinds of carbon were formed on the Ni–Co catalyst, which has the higher metal content; one kind of carbon can be oxidized in air at 500 °C, and another kind can be oxidized at 600 °C. Correspondingly, Fig. 8d shows filamentous carbons of nanotubes with two very different diameters. However, there was no clear evidence that the nanotubes of different diameters were responsible for two TPO peaks.

Osaki et al. [51] related the carbon inhibition to the metal ensemble in catalysts and concluded that smaller ensembles are able to suppress carbon formation. On the other hand, Rostrup-Nielsen [41] observed that large nickel clusters are susceptible to carbon formation. From TEM pictures (Figs. 8a and 8b), it can be seen that the particle size is smaller on Ni–Co (L) than on Ni–Co. CO chemisorption was then carried out to measure the metal dispersion of Ni–Co bimetallic catalysts. For the bimetallic catalyst with the higher Ni–Co content, the metallic surface area was 4.1 m^2/g, and metal dispersion was 7.5%. The Ni–Co

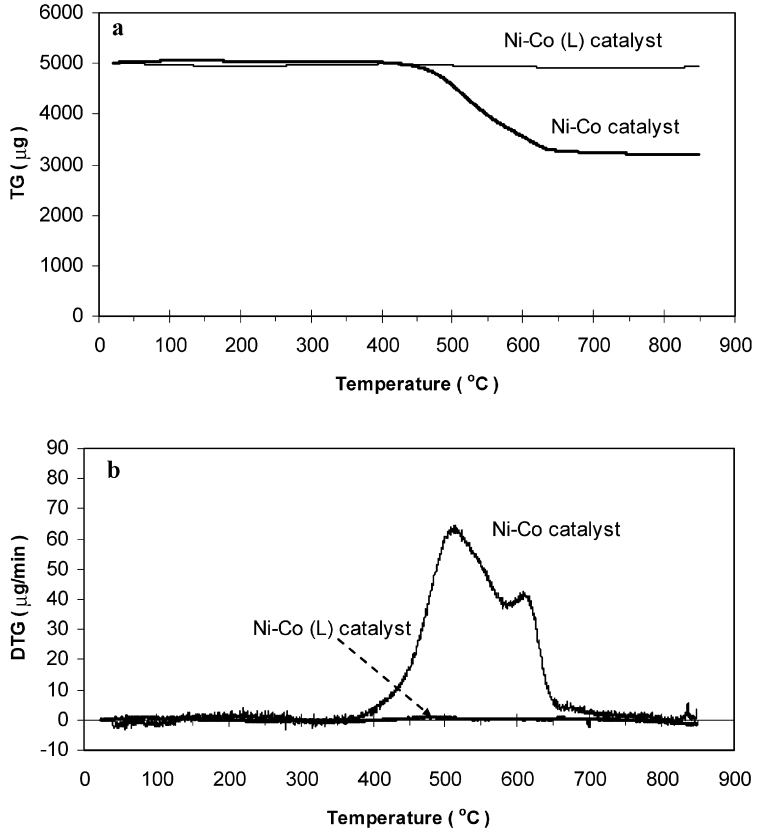

Fig. 7. Carbon formation on the different Ni–Co content bimetallic catalysts after 250 h reaction at: $T = 750\,^{\circ}C$, $P = 1$ atm, $F = 5.5$ L/h, $CH_4/CO_2/N_2 = 1/1/1$, 0.03 g catalyst. (a) TG profiles; (b) DTG profiles.

(L) catalyst had a lower metallic surface area (2.9 m^2/g) but a higher metal dispersion (8.8%) (Table 3). The higher metallic surface of the catalyst with the higher Ni–Co content led to the higher initial activity (Fig. 6); however, its lower metal dispersion and larger ensembles possibly resulted in rapid carbon formation and activity decay (Figs. 6 and 7). The excellent carbon resistance of Ni–Co (L) catalyst might be attributed to its higher metal dispersion and smaller metal ensembles.

3.2. Characterization of catalysts

3.2.1. Active metal composition

To gain insight into the relationship between catalyst properties and performance, comparative investigations were carried out over Ni or Co monometallic catalysts and Ni–Co (L) bimetallic catalyst. In the monometallic catalysts, Ni content or Co content was at the same level as the overall Ni and Co content in the bimetallic Ni–Co (L) catalyst, so that the comparison of catalytic performance could be made on the similar total active metal loading base. Bulk elemental composition was analyzed using ICP-MS, and surface elemental composition was determined by XPS. The results are given in Table 2. Comparison between surface composition and bulk composition indicated that $Ni_{surface}/Ni_{bulk}$ was 1.10 in the Ni monometallic catalyst and 1.19 in the bimetallic catalyst. $Co_{surface}/Co_{bulk}$ was 0.80 in the Co monometallic catalyst and 1.27 in the Ni–Co bimetallic catalyst. The coexistence of Ni–Co in the bimetallic catalyst made Co an apparent surface enrichment.

3.2.2. Reducibility

Hydrogen temperature-programmed reduction (H_2-TPR) experiments were conducted to investigate the reducibility of the catalysts. The TPR profiles are shown in Fig. 9. Accordingly, the reduction peaks in the ranges of 750–950 and 700–950 °C for the Ni and Co monometallic catalysts, respectively, corresponded to the reduction of Ni in a mixed spinel-phase $Ni_xMg_{1-x}Al_2O_4$ [52] and Co in a mixed spinel-phase $Co_xMg_{1-x}Al_2O_4$ [53]. The reduction peak in Ni–Co (L) bimetallic catalyst between 700 and 940 °C probably resulted from the reduction of Ni and Co in a very complex quaternary spinel-like phase [54]. In the high-temperature calcination process, Ni and Co also can form a continuous row of $Ni_xCo_{3-x}O_4$ spinels, $x > 0$ [55]. The reduction peak maximum of Ni–Co (L) bimetallic catalyst occurred at a lower temperature (850 °C) than those for Ni monometallic catalyst (868 °C) and Co monometallic catalyst (896 °C). This can be attributed in part to the surface enrichment of Ni and Co in the Ni–Co (L) catalyst, because Ni and Co atoms on the catalyst surface are more readily accessible than those in the bulk structures. In addition, the reduction of Ni–Co (L) bimetallic catalyst appeared to be a single reduction peak, which might indicate formation of the Ni–Co alloy during reduction. Rinkowski et al. [56] re-

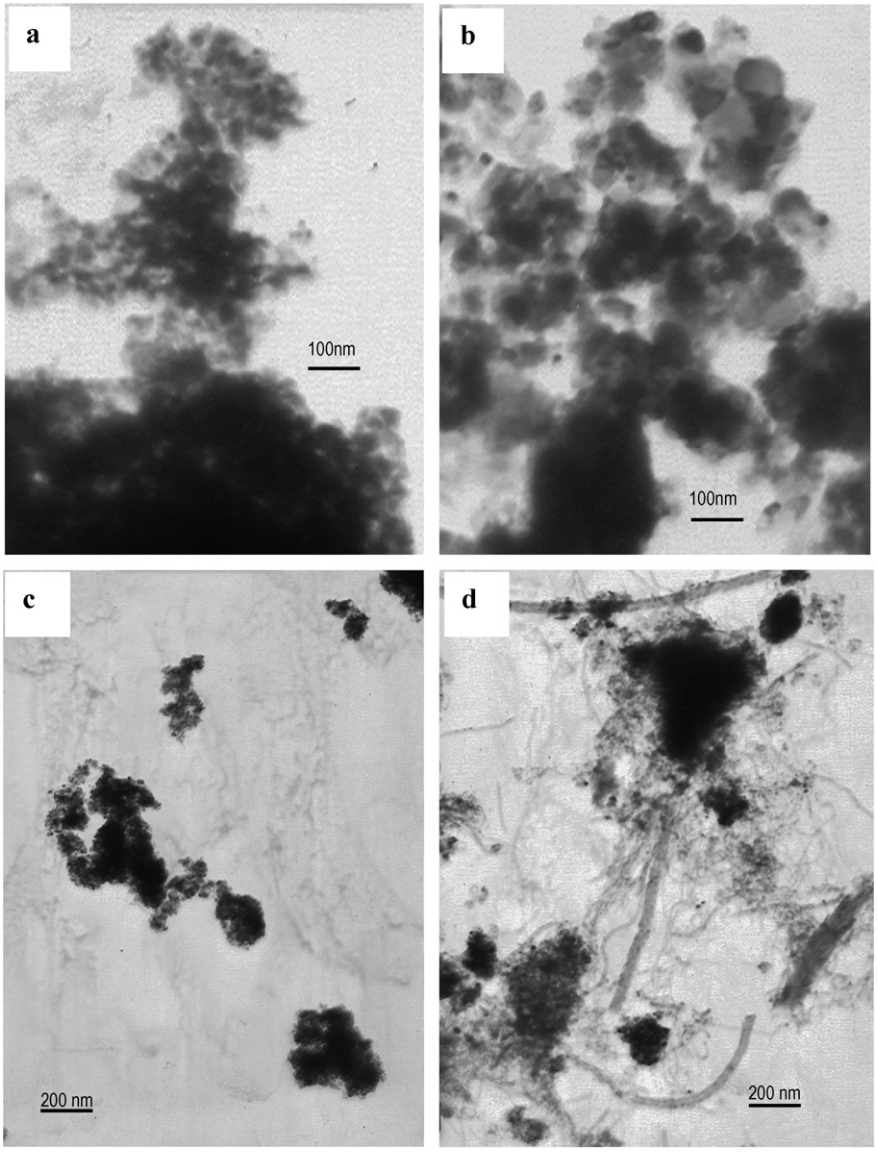

Fig. 8. TEM micrographs of catalysts before and after 250 h reaction at conditions: $T = 750\,^{\circ}C$, $P = 1$ atm, $F = 5.5$ L/h, $CH_4/CO_2/N_2 = 1/1/1$, 0.03 g catalyst. (a) Ni–Co (L) before reaction; (b) Ni–Co before reaction; (c) Ni–Co (L) after 250 h reaction; (d) Ni–Co after 250 h reaction.

ported that one-stage reduction of bimetallic catalysts illustrates the alloying of metals in the reduction process.

3.2.3. Bulk phases

XRD analysis was used to identify the bulk phase property of the catalysts. As shown in Fig. 10, spinel phases and MgO-type phases were observed in all the three samples. No apparent difference was revealed between the XRD patterns of Ni–Co (L) bimetallic catalyst and Ni or Co monometallic catalyst. According to Tichit et al. [52–54], Ni^{2+}, Co^{2+}, Mg^{2+}, and Al^{3+} belong to the same lattice in the Ni/Co/Al/Mg composite catalysts. A high calcination temperature favors the formation of Ni^{2+}–Al^{3+}, Co^{2+}–Al^{3+}, and Mg^{2+}–Al^{3+} solid solutions of spinel type and of the stoichiometric $NiAl_2O_4$, $CoAl_2O_4$, and $MgAl_2O_4$ spinel phases [52–54]. The Ni^{2+}–Co^{3+} spinel-type solid solution and $NiCo_2O_4$ spinel also can be formed at high calcination temperatures [55]. These spinel-type solid solution phases and spinel phases in the catalysts are indistinguishable by XRD (Fig. 10) due to their similarity. This result is understandable, because the major components of the catalysts are Al and Mg, which could form similar solid structures from identical preparation processes.

3.2.4. Oxidation states of Ni and Co

Fig. 11 shows that, based on XPS analysis, Ni^{2+} (854 and 860 eV) [57] was predominant in the Ni monometallic catalyst, and Co^{3+} (777 eV) [58] was present in large amounts in the Co monometallic catalyst. However, other oxidation states for both metals, such as Ni^{3+} and Co^{2+}, increased in the Ni–Co (L) bimetallic catalyst. It is interesting to note that part of the Ni shifted from a lower oxidation state to a higher oxidation state, and part of the Co shifted from a higher to a lower oxidation state. This indicates an electron transfer between Ni and Co in the bimetallic catalyst, which is believed to protect metal from

oxidation during the reaction [25]. This further confirms the near-distance interaction between the two metal atoms, which may easily form Ni–Co alloy on the catalyst surface during reduction.

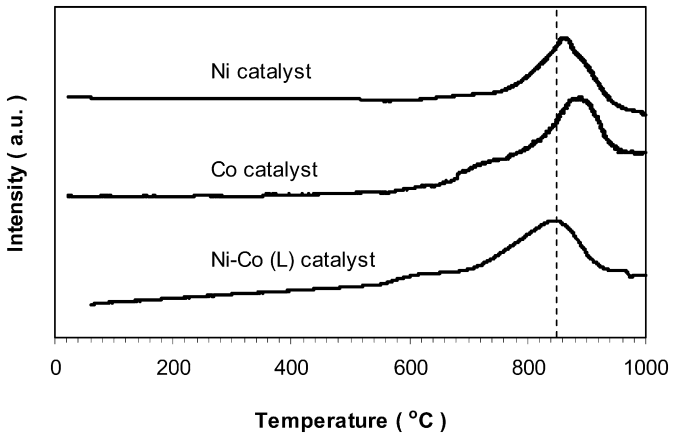

Fig. 9. TPR profiles of Ni and Co monometallic and Ni–Co (L) bimetallic catalysts calcined at 900 °C.

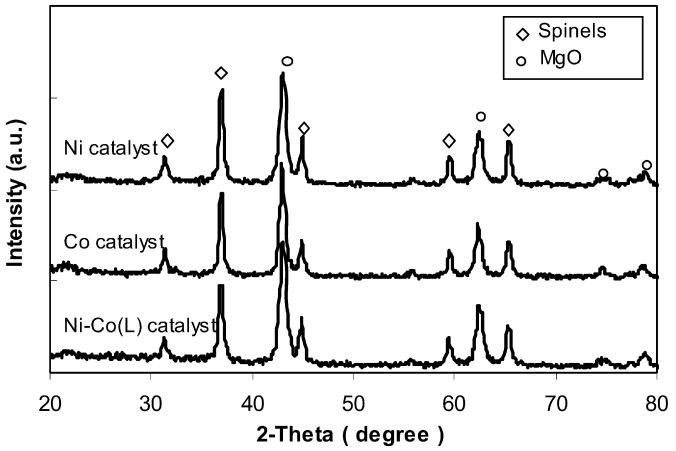

Fig. 10. XRD analysis of Ni and Co monometallic and Ni–Co (L) bimetallic catalysts calcined at 900 °C.

3.3. Catalyst activity, stability, and carbon resistance

Initial catalyst activity has a direct correlation with active metal content. This is why the Ni–Co bimetallic catalyst with higher Ni–Co content had higher initial activity than the Ni–Co (L) catalyst (Fig. 6). However, comparing the activity for monometallic and bimetallic catalysts showed that the synergy between Ni and Co made a significant difference. Table 4 and Fig. 12 show the test results of the Ni and Co monometallic catalysts and the Ni–Co (L) bimetallic catalyst at 750 °C, 1 atm, $F = 5.5$ L/h, $CH_4/CO_2/N_2 = 1/1/1$, and 0.025 g of catalyst. The Ni and Co monometallic catalysts seemed to have similar performance, with no significant differences in either activity or carbon formation over the two monometallic catalysts. Ni–Co (L) bimetallic catalyst, on the other hand, had higher activity and no detectable carbon formation. This synergistic phenomenon of the two active metals has been reported by others as well. Becerra et al. [59] reported that the combination of Ru and Ni significantly improved the catalyst activity for carbon dioxide reforming of methane as a result of the increased number of metal surface atoms. Rinkowski et al. [56] observed that the surface metal atoms are enriched in the Ni–Pt bimetallic system due to Ni surface enrichment. Along with the active metal content on the catalyst surface, metal dispersion and degree of catalyst reduction are important factors affecting catalyst activity [60]. The metal dispersion had been enhanced by the synergy of Ni–Co in bimetallic catalyst (Table 3). The degree of catalyst reduction was likely increased, as confirmed by the lower temperature of the reduction peak maximum and larger peak area of Ni–Co (L) (Fig. 9).

Compared with the Ni and Co monometallic catalysts, the Ni–Co (L) bimetallic catalyst showed not only higher activity, but also better stability and carbon resistance (Table 4 and Fig. 12). Fig. 12 clearly shows that the activity of Ni and Co monometallic catalysts dropped during the 28-h stability test, but the activity of Ni–Co (L) bimetallic catalyst stayed the same as its initial value. TG analysis revealed that Ni and Co monometallic catalysts had relatively the same carbon formation rate (0.003186 and 0.003973 g_c/g_{cat}-h, respectively), but

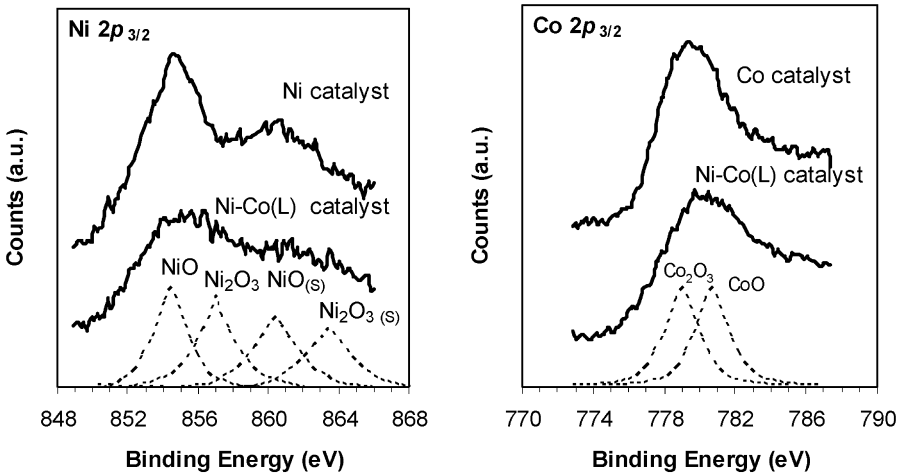

Fig. 11. XPS spectra of Ni $2p_{3/2}$ and Co $2p_{3/2}$ in Ni and Co monometallic and Ni–Co (L) bimetallic catalysts calcined at 900 °C.

Table 4
Activity and carbon formation rate of Ni and Co monometallic and Ni–Co (L) bimetallic catalysts

Catalyst	Initial conversion (%)		Final conversion (%)		Average carbon formation rate (g_c/g_{cat}-h)
	CH_4	CO_2	CH_4	CO_2	
Ni	62.9	73.4	58.0	69.5	0.003186
Co	67.6	77.0	58.3	71.2	0.003973
Ni–Co (L)	83.8	87.0	83.9	87.1	0

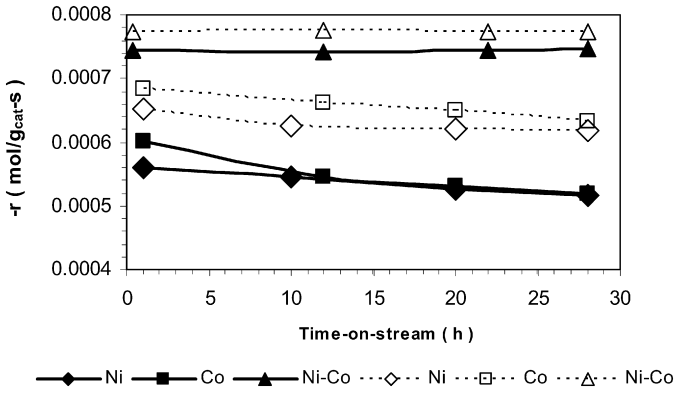

Fig. 12. Comparison of stability of Ni–Co (L) bimetallic catalyst and Ni and Co monometallic catalysts (solid line: CH_4 reaction rate; dotted line: CO_2 reaction rate). Reaction conditions: $T = 750\,^{\circ}C$, $P = 1$ atm, $F = 5.5$ L/h, $CH_4/CO_2/N_2 = 1/1/1$, 0.025 g catalyst.

the Ni–Co (L) bimetallic catalyst had no detectable carbon formation (Table 4). Carbon formation appeared to be the major reason for catalyst deactivation for the monometallic catalysts. Bradford and Vannice [13] reported that inactive carbon in the form of filamentous whiskers was primarily responsible for the catalyst deactivation. TEM analysis showed such filamentous whiskers were formed on the higher Ni–Co content bimetallic catalyst. The good stability of the Ni–Co (L) catalyst can be ascribed to its high carbon resistance.

Different authors attributed carbon resistance to different properties. Ruckenstein and Hu [17,18] attributed the stability and carbon resistance of NiO/MgO to the formation of a solid solution between NiO and MgO. Zhang et al. [34] and Chang et al. [35] reported that promoting the basicity of catalysts by adding K and Ca enhanced the adsorption of CO_2 and thus suppressed carbon formation. Other studies [61–63] have indicated that high carbon resistance was due to the strong metal–support interaction (SMSI). In our case, we believe that formation of solid solutions occurred in both the bimetallic catalyst and the monometallic catalysts (Fig. 10). The TPR profiles indicate that the bimetallic catalysts had SMSI, confirming the findings of previous studies [61–64]. Our monometallic and bimetallic catalysts had no basicity, as demonstrated by CO_2-TPD. (TPD results are not shown, because all CO_2-TPD profiles were flat lines without any CO_2-desorption peaks.) Comparing the carbon resistance of the Ni–Co (L) bimetallic catalyst and the Ni and Co monometallic catalysts leads us to believe that the excellent carbon resistance of Ni–Co (L) is resulted from the synergy of Ni and Co, better metal dispersion, and smaller metal ensembles. In addition, the formation of various spinel-type solid solutions, the SMSI, and the good sintering resistance of MgO phases also contributed to the high catalytic activity and excellent carbon resistance.

4. Conclusion

Ni–Co bimetallic catalysts composed by coprecipitating Ni-, Co-, Al-, and Mg-containing precursor solutions demonstrate excellent performance for carbon dioxide reforming of methane. The synergy of Ni and Co in the bimetallic catalysts provides not only high activity, but also very good carbon resistance, and thus creates catalysts with outstanding stability. Comparative studies conducted with Ni and Co monometallic catalysts and Ni–Co bimetallic catalyst show that the superior performance of Ni–Co catalysts comes from the synergetic effect, good metal dispersion, high metallic surface, formation of different types of solid solutions, and SMSI.

Acknowledgments

The authors gratefully acknowledge financial support from the Natural Science and Engineering Research Council of Canada (NSERC) and the Canada Foundation for Innovation (CFI).

References

[1] R. Burch, M.I. Petch, Appl. Catal. 88 (1992) 39.
[2] E.C. Alyea, J. Wang, Appl. Catal. 104 (1993) 77.
[3] F. Fischer, H. Tropsch, Brennst. Chem. 9 (1928) 39.
[4] T.A. Chubb, Sol. Energy 24 (1980) 341.
[5] D. Fraenkel, R. Levitan, M. Levy, Int. J. Hydrogen Energy 11 (1986) 267.
[6] J.T. Richardson, S.A. Paripatyadar, Appl. Catal. 61 (1990) 293.
[7] M. Levy, R. Levitan, E. Meirovitvh, A. Segal, H. Rosin, R. Rubin, Sol. Energy 48 (1992) 395.
[8] M. Levy, R. Levitan, H. Rosin, R. Rubin, Sol. Energy 50 (1993) 179.
[9] J.T. Richardson, M. Garrait, J.-K. Hung, Appl. Catal. A 255 (2003) 69.
[10] U.L. Portugal, A. Santos, S. Damyanova, C. Marques, J. Bueno, J. Mol. Catal. 184 (2002) 311.
[11] A. Erdohelyi, J. Cserenyi, F. Solymosi, J. Catal. 141 (1993) 287.
[12] J.R. Ostrupnielsen, J.H.B. Hansen, J. Catal. 144 (1993) 38.
[13] M.C.J. Bradford, M.A. Vannice, Catal. Rev. Sci. Eng. 41 (1999) 1.
[14] J.R. Rostrup-Nielsen, Catal. Today 37 (1997) 225.
[15] A. Slagtern, U. Olsbye, R. Blom, I.M. Dahl, Stud. Surf. Sci. Catal. 107 (1997) 497.
[16] A.T. Ashcroft, A.K. Cheetham, M.L.H. Green, P.D.F. Vernon, Nature 352 (1991) 225.
[17] E. Ruckenstein, Y.H. Hu, Appl. Catal. A 133 (1995) 149.
[18] Y.H. Hu, E. Ruckenstein, Catal. Lett. 36 (1996) 145.
[19] K. Tomishige, Y. Himeno, Y. Matsuo, Y. Yoshinaga, K. Fujimoto, Ind. Eng. Chem. Res. 39 (2000) 1891.
[20] J.B. Wang, L.-E. Kuo, T.-J. Huang, Appl. Catal. A 249 (2003) 93.
[21] H.B. Zhang, P. Chen, G.-D. Lin, K.-R. Tsai, Appl. Catal. A 166 (1998) 343.

[22] J.-S. Choi, K.-I. Moon, Y.G. Kim, J.S. Lee, C.-H. Kim, D.L. Trimm, Catal. Lett. 52 (1998) 43.
[23] D.L. Trimm, Catal. Today 37 (1997) 225.
[24] V.R. Choudhary, A.S. Mamman, J. Chem. Technol. Biotechnol. 73 (1998) 345.
[25] K. Takanabe, K. Nagaoka, K. Nariai, K.-I. Aika, J. Catal. 232 (2005) 268.
[26] J.H. Sinfelt, Bimetallic Catalysts: Discovery, Concepts and Applications, Wiley, New York, 1983.
[27] V. Ponec, G.C. Bond, Catalysis by Metals and Alloys, Elsevier, Amsterdam, 1995.
[28] J.A.C. Dias, J.M. Assaf, Catal. Today 85 (2003) 59.
[29] S.H. Seok, S.H. Choi, E.D. Park, S.H. Han, J.S. Lee, J. Catal. 209 (2002) 6.
[30] T. Osaki, T. Mori, J. Catal. 204 (2001) 89.
[31] C.E. Quincoces, S. Dicundo, A.M. Alvarez, M.G. Gonzalez, Mater. Lett. 50 (2001) 21.
[32] C.E. Quincoces, S.P.D. Vargas, P. Grange, M.G. Gonzales, Mater. Lett. 56 (2002) 698.
[33] F. Frusteri, F. Arena, G. Calogero, T. Torre, A. Parmaliana, Catal. Commun. 2 (2001) 49.
[34] Z.L. Zhang, X.E. Verykios, Catal. Today 21 (1994) 589.
[35] J.-S. Chang, S.-E. Park, H. Chon, Appl. Catal. A 145 (1996) 111.
[36] T. Horiuchi, K. Sakuma, T. Fukui, Y. Kubo, T. Osaki, T. Mori, Appl. Catal. A 144 (1996) 111.
[37] O. Yamazaki, T. Nozaki, K. Omata, K. Fujimoto, Chem. Lett. (1992) 1953.
[38] J.T. Richardson, Principles of Catalyst Development, Plenum, New York/London, 1989, pp. 1–48.
[39] J.M. Thomas, W.J. Thomas, Introduction to the Principles of Heterogeneous Catalysis, Academic Press, London/New York, 1967, pp. 180–239.
[40] J.H. Edwards, A.M. Maitra, Fuel Process. Technol. 42 (1995) 269.
[41] J.R. Rostrup-Nielsen, J. Catal. 33 (1974) 184.
[42] J.R. Rostrup-Nielsen, Stud. Surf. Sci. Catal. 36 (1988) 73.
[43] J.T. Richardson, Principles of Catalyst Development, Plenum, New York/London, 1989, p. 29.
[44] S. Seok, S. Han, J. Lee, Appl. Catal. A 215 (2001) 31.
[45] S. Tang, L. Ji, J. Lin, H.C. Zeng, K.L. Tan, K. Li, J. Catal. 194 (2000) 424.
[46] J.-M. Wei, B.-Q. Xu, J.-L. Li, Z.-X. Cheng, Q.-M. Zhu, Appl. Catal. A 196 (2000) L167.
[47] E. Ruckenstein, Y.H. Hu, J. Catal. 162 (1996) 230.
[48] Z.L. Zhang, X.E. Verykios, Appl. Catal. A 138 (1996) 109.
[49] Z.L. Zhang, X.E. Verykios, S.M. MacDonald, S.A. Affrossman, J. Phys. Chem. 100 (1996) 744.
[50] V.A. Tsopiroaro, X.E. Verykios, Catal. Today 64 (2001) 83.
[51] T. Osaki, T. Mori, J. Catal. 204 (2001) 89.
[52] D. Tichit, F. Medina, B. Coq, R. Dutartre, Appl. Catal. A 159 (1997) 241.
[53] S. Ribet, D. Tichit, B. Coq, B. Ducourant, F. Morato, J. Solid State Chem. 142 (1999) 382.
[54] B. Coq, D. Tichit, S. Ribet, J. Catal. 189 (2000) 117.
[55] K. Petrov, G. Will, J. Mater. Sci. Lett. 6 (1987) 1153.
[56] J.M. Rihkowski, T. Paryjczak, M. Lenik, M. Farbotko, J. Goralski, J. Chem. Soc. Faraday Trans. 91 (1995) 3481.
[57] J.K. Kang, S. Rhee, Thin Solid Films 391 (2001) 57.
[58] J.F. Marco, J.R. Gancedo, J. Ramon, M. Gracia, J.L. Gantier, J. Mater. Chem. 11 (2001) 3087.
[59] A. Becerra, M.E. Iriarte, M. Dimitrijewit, A. Castro-Luna, Bol. Soc. Chil. Quím. 47 (2002) 385.
[60] B.S. Liu, C.T. Au, Appl. Catal. A 244 (2003) 181.
[61] Y.-G. Chen, K. Tomishige, K. Yokoyama, K. Fujimoto, J. Catal. 184 (1999) 79.
[62] L. Ji, S. Tang, H.C. Zeng, J. Lin, K.L. Tan, Appl. Catal. A 207 (2001) 247.
[63] S. Wang, G.Q.M. Lu, Appl. Catal. B 16 (1998) 269.
[64] I.Y. Ahn, W.J. Kim, S.H. Moon, Appl. Catal. A 308 (2006) 75.